



A tight squeeze: geometric effects on the performance of three-electrode electrochemical-aptamer based sensors in constrained, in-vivo placements

Journal:	<i>Analyst</i>
Manuscript ID	AN-ART-12-2022-002096.R1
Article Type:	Paper
Date Submitted by the Author:	27-Jan-2023
Complete List of Authors:	<p>Leung, Kaylyn; University of California Santa Barbara, Department of Chemistry and Biochemistry Gerson, Julian; University of California Santa Barbara, Department of Psychological and Brain Sciences Emmons, Nicole; University of California Santa Barbara, Department of Psychological and Brain Sciences Roehrich, Brian BR; University of California Santa Barbara, Chemistry and Biochemistry Verrinder, Elsi ; University of California Santa Barbara, Department of Chemistry and Biochemistry Fetter, Lisa; University of California Santa Barbara, Biomolecular Sciences and Engineering Kippin, Tod E.; University of California Santa Barbara, Psychological and Brain Sciences; University of California Santa Barbara, Molecular Cellular and Developmental Biology; University of California Santa Barbara, Neuroscience Research Institute Plaxco, Kevin; University of California Santa Barbara, Chemistry and Biochemistry</p>

1
2
3 **A tight squeeze: geometric effects on the performance of three-electrode electrochemical-**
4 **aptamer based sensors in constrained, in-vivo placements**
5
6

7 Kaylyn K. Leung^{1,5}, Julian Gerson^{2,5}, Nicole Emmons^{2,5}, Brian Roehrich¹, Elsi Verrinder^{1,5}, Lisa
8 Fetter^{3,5}, Tod Kippin^{2,4}, and Kevin W. Plaxco^{1,3,5*}
9
10

11
12 ¹Department of Chemistry and Biochemistry, University of California Santa Barbara, Santa
13 Barbara, CA 93106, USA.

14 ²Department of Psychological and Brain Sciences, University of California, Santa Barbara, CA
15 93106, USA.

16 ³Biomolecular Sciences and Engineering, University of California, Santa Barbara, California
17 93106, United States

18 ⁴Department of Molecular Cellular and Developmental Biology, University of California, Santa
19 Barbara, CA 93106, USA.

20 ⁵Center for Bioengineering, University of California Santa Barbara, Santa Barbara, CA 93106,
21 USA.
22

23
24
25
26
27 *Corresponding author. Email: kwp@ucsb.edu
28

29
30 **Keywords:** Electrochemical sensor, Aptamer sensor, Sensor engineering, Sensor Design
31
32
33
34
35
36
37
38
39
40
41
42
43
44
45
46
47
48
49
50
51
52
53
54
55
56
57
58
59
60

Abstract

Electrochemical, aptamer-based (EAB) sensors are the first molecular monitoring technology that is (1) based on receptor binding and not the reactivity of the target, rendering it fairly general, and (2) able to support high-frequency, real-time measurements in situ in the living body. To date, EAB-derived in-vivo measurements have largely been performed using three electrodes (working, reference, counter) bundled together within a catheter for insertion into the rat jugular. Exploring this architecture, here we show that the placement of these electrodes inside or outside of the lumen of the catheter significantly impacts sensor performance. Specifically, we find that retaining the counter electrode within the catheter increases the resistance between it and the working electrode, increasing the capacitive background. In contrast, extending the counter electrode outside the lumen of the catheter reduces this effect, significantly enhancing the signal-to-noise of intravenous molecular measurements. Exploring counter electrode geometries further, we find that they need not be larger than the working electrode. Putting these observations together, we have developed a new intravenous EAB architecture that achieves improved performance while remaining short enough to safely emplace in the rat jugular. These findings, though explored here with EAB sensors may prove important for the design of many electrochemical biosensors.

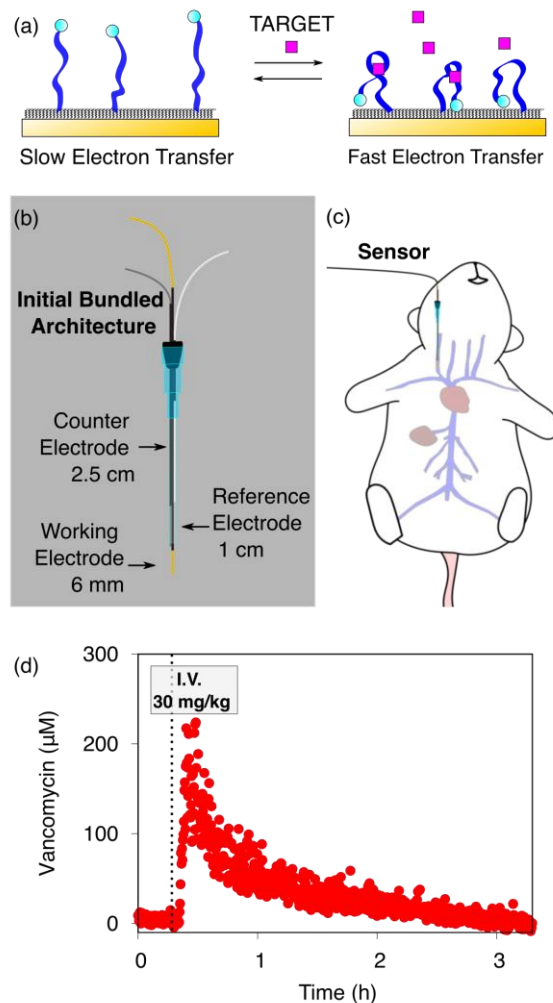
Introduction

The ability to measure the concentrations of clinically relevant molecular targets continuously and in real time in the living body would significantly advance our ability to diagnose, monitor, treat, and understand disease. Towards this goal, we are developing electrochemical aptamer-based (EAB) sensors: a reagentless, reversible molecular sensing platform that performs well in vivo. In these, the binding of a specific target induces a conformational change in an electrode-attached, redox-reporter-modified aptamer (Fig. 1a), resulting in an easily detectable change in the redox reporter's electron transfer kinetics that we typically monitor using square wave voltammetry¹⁻⁶. Because this conformation-linked signaling mechanism does not rely on any specific chemical or enzymatic reactivity of the target itself, the development of EAB sensors against new targets is relatively easy. With this signal transduction mechanisms that mimics those found in naturally occurring chemoperception systems, EAB sensors also support real-time, high-frequency measurements in complex sample matrices, including unprocessed bodily fluids.^{2,7-10} Building on these advantages, EAB sensors have already been used to measure the rise and fall of more than a half-dozen therapeutics^{1,2,6,11}, drugs of abuse, and metabolites⁵ in real time in the blood of live rats. The resulting high-frequency, real-time molecular measurements have even been shown to support closed-loop, feedback-controlled drug delivery;^{1,12} an advance that could usher in a new era in which pharmacological therapies can be delivered with unprecedented precision.¹³

In our prior work, we have deployed in-vivo EAB sensors as a 3-electrode system consisting of a gold wire working electrode modified with the target-recognizing aptamer, a chloride-anodized silver wire reference electrode (RE), and a platinum wire counter electrode (CE). These are individually insulated using heat-shrink polytetrafluoroethylene (PTFE) and then bundled together in a staggered fashion and placed in a catheter. To date, we have published work with in-vivo EAB sensors using two specific arrangements following this general scheme. In one, 75 μm diameter wires were used for all three electrodes and only the gold working electrode extends out of the catheter and into the vein.^{1,2,5,6,11,14} In a second, we employed 200 μm diameter wires placed in the catheter (Fig. 1b) such that half of the reference electrode and all of the working electrode extend out of the catheter and into the vein (Fig. 1c).¹⁵ In both cases, we retained the counter electrode

1
2
3 within the catheter, so as to reduce the length of the sensor and thus avoid interfering with the
4 heart.
5
6
7

8
9 As extensive prior literature demonstrates and as shown here, the in vivo EAB architectures we
10 have employed support unprecedentedly highly-time resolved measurements of plasma drug and
11 metabolite levels (e.g., Fig. 1d). This said, however, several aspects of the fabrication of
12 intravenous EAB sensors remain unexamined, suggesting that their performance could be further
13 improved. Specifically, here we explore the extent to which the relative placement of the three
14 electrodes in an intra-catheter EAB sensor alters the device's performance, with the expectation
15 that better understanding this will guide us towards improved signal-to-noise ratios and smaller,
16 less invasive devices.
17
18
19
20
21
22
23
24



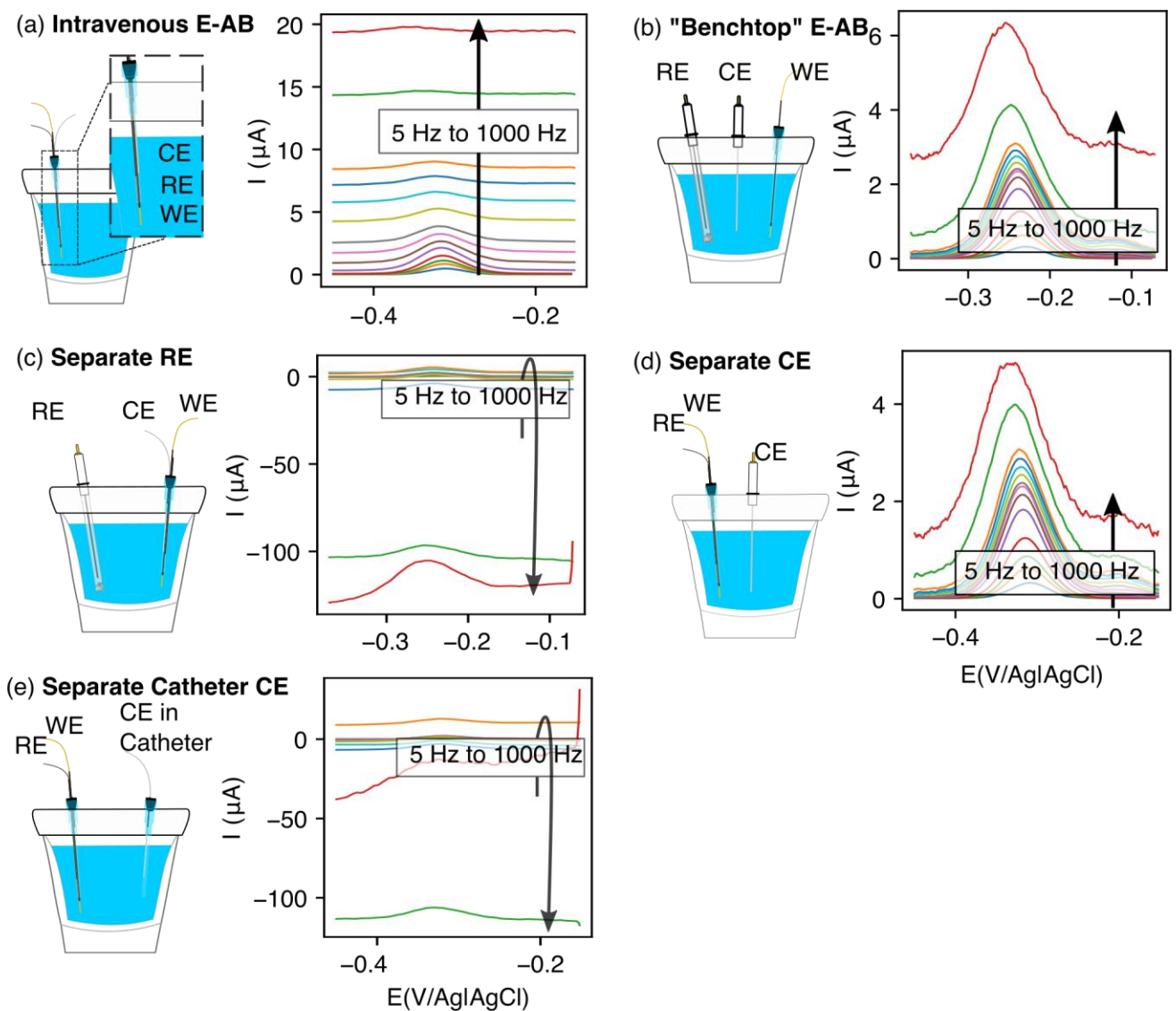
1
2
3
4
5 **Figure 1.** (a) Electrochemical aptamer-based (EAB) sensors are comprised of redox-reporter-
6 modified, conformation-shifting aptamers attached to a gold electrode via a self-assembled
7 monolayer. The phrase “conformation-shifting” refers to an aptamer that has been
8 reengineered such that target binding reversibly alters its shape, changing in turn the rate of
9 electron transfer of the attached redox reporter. (b) EAB sensors support molecular
10 measurements in vivo. To do so in the rat jugular, we have used bundled, catheter-enclosed
11 sensors. In one architecture, for example, a gold wire working electrode, a platinum wire
12 counter electrode, and a chloride-anodized silver wire reference electrode are staggered within
13 a 20-gauge catheter such that the counter electrode remains within the catheter, and half of the
14 reference electrode and all of the working electrode extend into the lumen of the vein. (c) This
15 is then surgically inserted into the external jugular vein of an anesthetized rat. (d) Using this
16 and related architectures we have monitored the plasma concentrations of multiple drugs and
17 metabolites in live rats.^{1,2,5,6,11} Shown here, for example, are 14-s-resolved plasma vancomycin
18 measurements performed using the described architecture emplaced in the rat jugular after an
19 intravenous injection of the drug.
20
21
22
23
24
25
26

27 **Results and discussion**

28
29
30 The performance of EAB sensors depends strongly on whether their electrodes are placed inside
31 or outside of a catheter. To see this, we first used in vitro experiments to compare a “bundled-
32 electrodes” intravenous architecture, in which the counter and reference electrodes are retained
33 within a catheter and the working electrode extends out of the lumen, with a sensor comprised of
34 three physically separated, catheter-free electrodes. Doing so, we find that the baseline currents
35 associated with the bundled architecture are (1) high and (2) a relatively strong function of square
36 wave frequency (Fig. 2a). This behavior contrasts with that seen in the “benchtop” E-AB sensor
37 where the reference and counter electrodes are separated from the bundle (Fig. 2b). The high
38 baselines associated with the bundled sensor reduce the peak currents, suggesting the details of the
39 placement of EAB electrodes within a catheter may harm sensor performance.
40
41
42
43
44
45
46
47

48
49 We next set out to determine which of the three electrodes in an EAB sensor are responsible for
50 the high baseline currents associated with our initial bundled architecture. As our first experiment,
51 we characterized a sensor in which the counter and working electrodes were placed in the catheter,
52 but the reference electrode (here a commercial, glass-frit Ag/AgCl reference) was physically
53 separated. Under these conditions, the baseline currents we observe are as high and as strongly
54
55
56
57
58
59
60

1
2
3 frequency dependent as those seen with the initial bundled architecture (Fig. 2c). Following this,
4 we separated the counter electrode, leaving the reference and the working electrode in the catheter.
5 With this case, we recover the low baselines and reduce the frequency dependence observed for
6 the separated electrodes architecture (Fig. 2d). Building on these observations, we next separated
7 the counter electrode but placed it in a second catheter. The baseline currents we observed for this
8 architecture were again as high and as strongly frequency dependent as those of the initial bundled
9 architecture (Fig. 2e).



10
11
12
13
14
15
16
17
18
19
20
21
22
23
24
25
26
27
28
29
30
31
32
33
34
35
36
37
38
39
40
41
42
43
44
45
46
47
48
49
50
51
52
53
54
55
56
57
58
59
60
Figure 2. The performance of EAB sensors is strongly dependent on which of their three electrodes are placed inside or outside of the catheter. (a) For example, our initial "bundled"

1
2
3 architecture, in which all of the working electrode and half of the reference electrode extend
4 out of a 20-gauge catheter but the counter electrode remains within, produces high and strongly
5 frequency dependent baseline currents. (b) In contrast, when we employ three, physically
6 separated electrodes (including, here, a commercial Ag/AgCl reference), the baseline is lower
7 and less frequency dependent. (c) When only the reference electrode is separated, the resulting
8 baselines are again strongly frequency dependent. (d) When we separate only the counter
9 electrode from the bundle, however, we recover the behavior seen for the fully separated
10 electrodes geometry. (e) Finally, when we place the separated counter electrode in a 20-gauge
11 catheter, the baselines once again become strongly frequency dependent.
12
13
14
15
16
17

18 The poorer performance seen when the counter electrode is placed inside a catheter arises due to
19 the high solution resistance this architecture produces. To see why this may be true, consider the
20 working principles of a 3-electrode electrochemical cell. In the absence of redox reactions, this
21 cell can be modeled as a series RC circuit comprised of a resistor of resistance R_s , which captures
22 the resistance of the solution between the working and counter electrodes, and a capacitor of
23 capacitance C_{dl} , which captures the capacitance of the electric double layer (Fig. 3a,b).¹⁶ How
24 rapidly the capacitor charges (i.e., the time it takes for the formation of the double layer) depends
25 on a time constant given by the product $R_s C_{DL}$. This, in turn, determines the current observed at a
26 specific time after the potential is applied, which defines the baseline current at a given square
27 wave frequency (in square wave voltammetry, the current is sampled at the end of each square
28 wave). Specifically, smaller time constants (i.e., faster charging) decrease the baseline current seen
29 at higher square wave frequencies (i.e., shorter time delays before current sampling). In contrast,
30 longer time constants increase the baseline currents. For architectures including a catheter-
31 enclosed counter electrode, the small cross section of the solution within the catheter ensures that
32 R_s is much larger, increasing the product $R_s C_{DL}$ and, in turn, the baseline currents increase
33 substantially as a function of square wave frequencies (Fig. 4a).
34
35
36
37
38
39
40
41
42
43
44
45
46
47
48
49
50
51
52
53
54
55
56
57
58
59
60

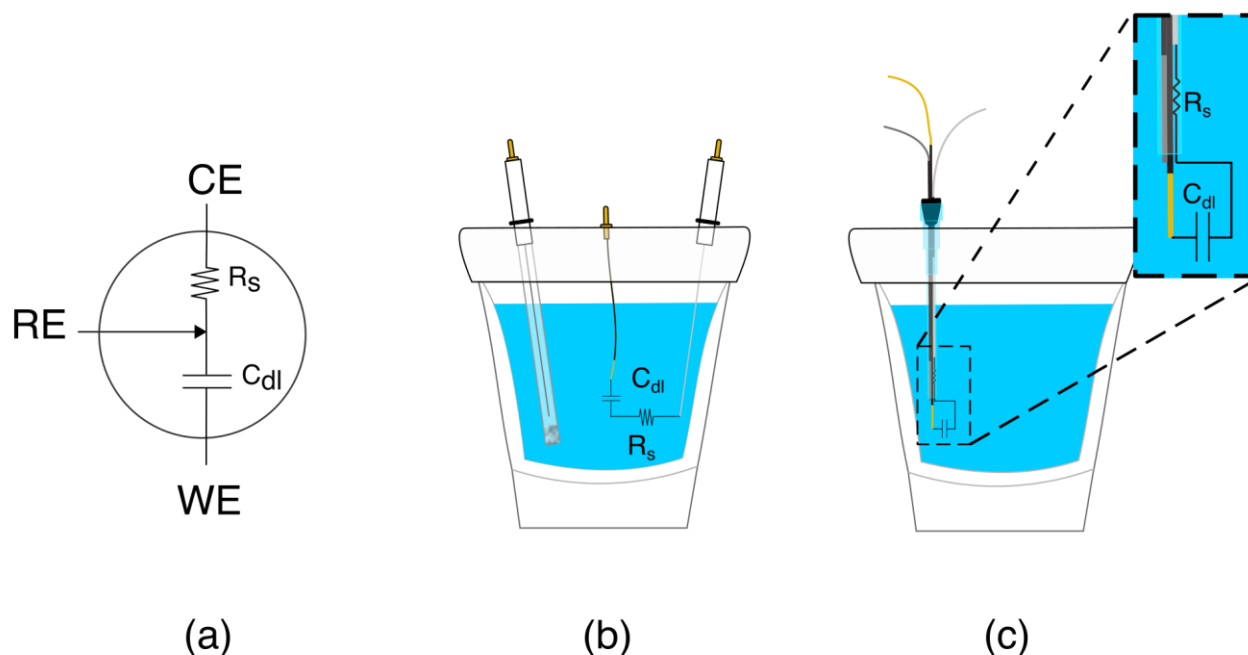


Figure 3. We can explain the differences in electrochemical behavior between the bundled and the separate sensor architectures by equating the electrochemical cell to an equivalent electrical circuit. (a) When no redox reactions are present, the RC circuit model can be used to describe a 3-electrode electrochemical system. (b) It consists of a capacitor representing the double layer at the working electrode interface (C_{dl}) and solution resistance (R_s) between the counter and working electrode. (c) For the bundled architecture, in which the counter electrode is retained within the catheter, the R_s between it and the working electrode is high due to limited thickness of the fluid layer within the catheter.

Characterization of our various sensor architectures using chronoamperometry and impedance spectroscopy supports the above conclusions. Specifically, using chronoamperometry to measure the sensor's temporal response to a potential jump we find that, as expected given the above arguments, the time constants observed when the counter electrode is free in solution are shorter than those seen when the counter electrode is contained within a catheter (Fig. 4b). Using electrochemical impedance to distinguish between the resistive components (arising due to R_s) and capacitive components (arising due to C_{dl}) of our sensors produces a similar picture.¹⁷ Specifically, R_s increases and C_{dl} is largely unchanged when we move the counter electrode from free in solution to constrained within a catheter. In a Nyquist plot, in which the imaginary impedance is plotted as a function of the real impedance (Fig. 4c), we find that the x intercept, which is indicative of R_s ,

is significantly higher when the counter electrode is inside the catheter than when it is outside. In contrast, the capacitive contributions remain unchanged (Table 1).

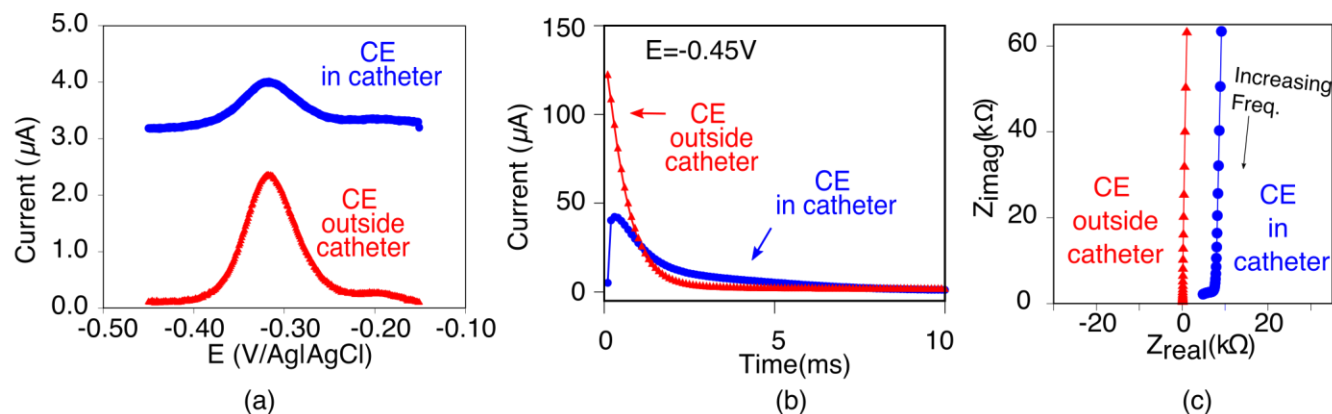
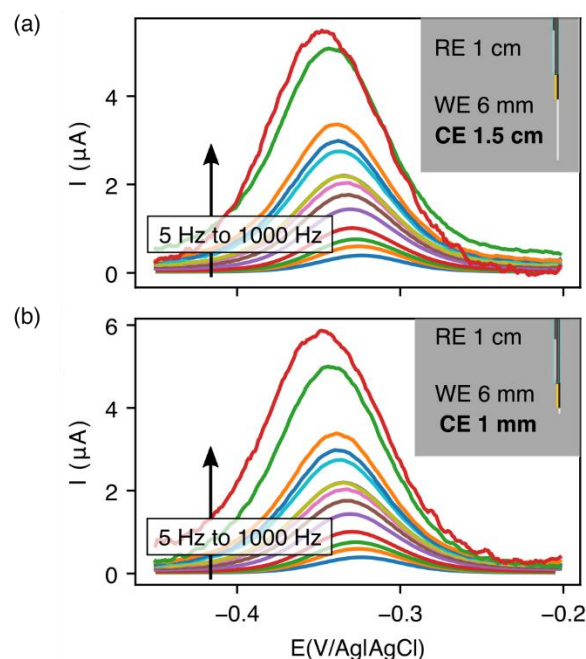


Figure 4. As evident with multiple electrochemical techniques, the electrochemical behavior of EAB sensors depends strongly on whether the counter electrode is positioned inside or outside of the catheter. (a) For example, employing square wave voltammetry (here at 100 Hz and 25 mV amplitude), the baseline current is significantly higher, and the peak height is smaller when the counter electrode is retained within the catheter (blue) versus when it is placed outside of the catheter (red). (b) In chronoamperometry, we apply a -0.45 V potential step and observe the resulting current transiently. When the counter electrode is placed inside the catheter (blue curve), the response time constant of the electrode is notably reduced. (c) Differences in the Nyquist plot seen when we characterized our architectures using electrochemical impedance spectroscopy further supports our arguments. Specifically, when the counter electrode is placed inside the catheter (blue curve), the x intercept, which indicates the solution resistance (R_s), increases 60-fold (table 1). In contrast, the increase in the imaginary impedance (on the y axis) is so similar for both cases resulting in C_{dl} values that are within error of one another (Table 1).

Table 1

Parameter	counter electrode inside the catheter	counter electrode outside the catheter
R_s	$6540 \pm 350 \Omega$	$104 \pm 4 \Omega$
C_{dl}	$0.49 \pm 0.02 \mu\text{F}$	$0.50 \pm 0.02 \mu\text{F}$
χ^2	1.0313	0.0091524

1
2
3 With our realization that sensor performance improves when the counter electrode is placed
4 outside the catheter, we next designed a 2nd bundled sensor architecture in which the reference
5 electrode is placed inside of the catheter and the counter and working electrodes both extend
6 beyond the catheter tip (Fig. 5). As noted above, however, a potential problem associated with
7 such architectures is that, using the 1.5 cm counter electrode length we usually employ, the bare
8 electrodes extend at least 2 cm beyond the catheter tip, risking interactions between the counter
9 electrode and the heart (Fig. 1c). Thus motivated, we next explored the extent to which we can
10 reduce the length of the exposed counter electrode without unduly degrading sensor performance.
11 To our surprise, given the generally held requirement for three electrode cells that the counter
12 electrode must be larger than the area of the working electrode,¹⁸⁻²⁰ we found no significant
13 differences in sensor performance when we shortened the counter electrode from 1.5 cm to 3 mm
14 (Fig. 5). We believe that this (to us unexpected) result arises due to the thiol passivating layer on
15 our working electrode, which reduces the double layer capacitance of the working electrode.
16 Irrespective of its origins, however, the practical upshot of this observation is that we can employ
17 a short enough counter electrode to ensure that the sensor does not reach the heart.
18
19
20
21
22
23
24
25
26
27
28
29
30



31
32
33
34
35
36
37
38
39
40
41
42
43
44
45
46
47
48
49
50
51
52 **Figure 5.** Reducing the counter electrode size by 15-fold does not significantly affect the
53 performance of EAB sensors. Specifically, we obtain near identical voltammograms whether using
54 a (a) 1.5 cm counter electrode or (b) one that is just 1 mm in length. For results at intermediate
55
56
57
58
59
60

1
2
3 counter electrode lengths, see Fig. S1. Insets illustrate the length of counter electrode exposed in
4 each geometry.
5
6

7 Building on the above observations we next designed an intravenous sensor architecture
8 employing a fully exposed, 6-mm-long counter electrode (Fig. 6a). Unfortunately, however, we
9 observed transient shorting when the potential was first applied to the sensor. We suspect that this
10 occurred because the tight fit of these wires inside the catheter leaves the PTFE shrink-tubing we
11 used to insulate the electrodes susceptible to microtears, leading to short-circuiting between the
12 reference and working electrodes. Fortunately, replacing the 200 μm diameter silver and 250 μm
13 diameter platinum wires with 125 μm diameter wires (Fig. 6a) eliminated this effect.
14
15
16
17
18
19
20
21
22
23
24
25
26
27
28
29
30
31
32
33
34
35
36
37
38
39
40
41
42
43
44
45
46
47
48
49
50
51
52
53
54
55
56
57
58
59
60

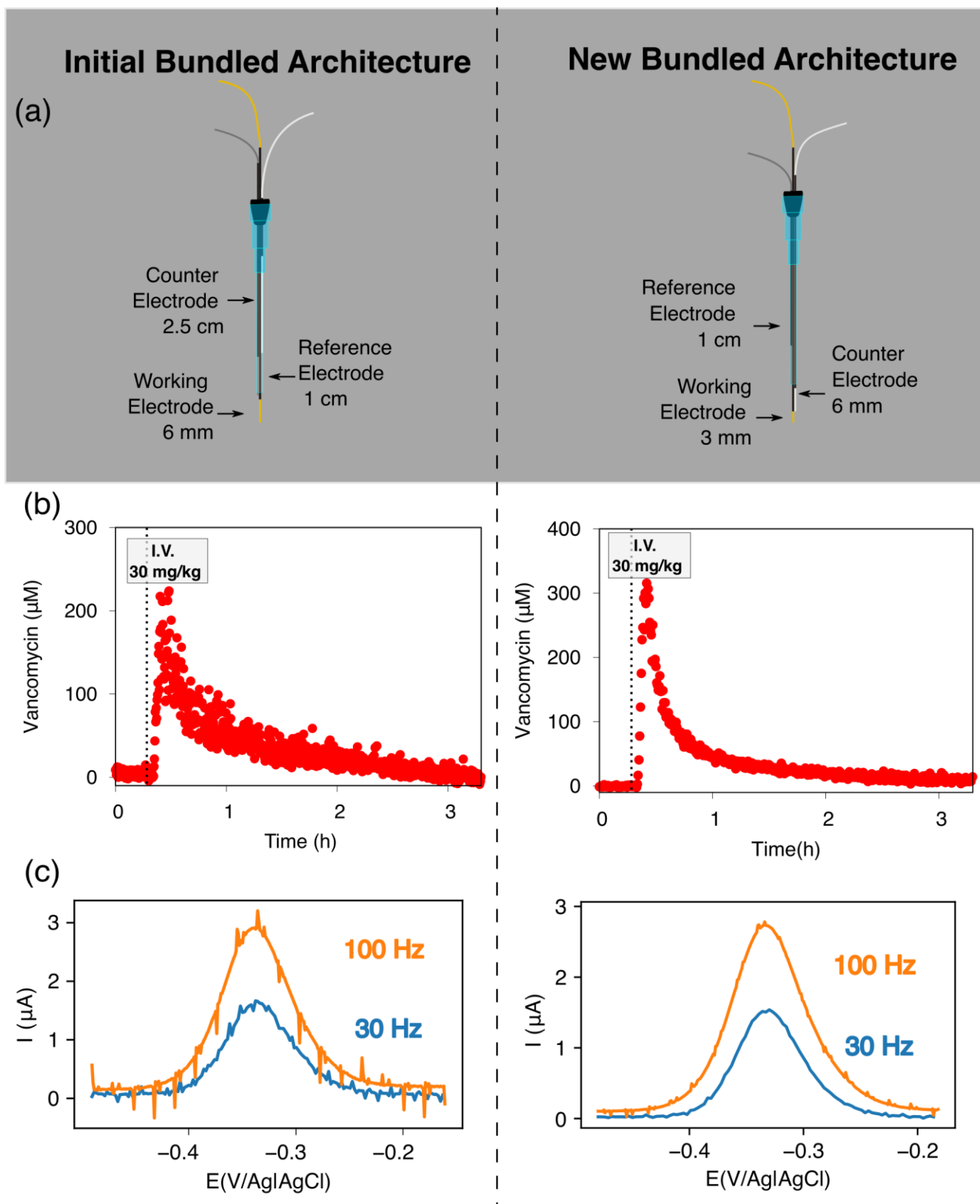


Figure 6. Building on the results reported here we have designed a new intravenous EAB architecture. (a) Altering the relative placement of the three electrodes to ensure that the counter

1
2
3 electrode is placed outside the catheter significantly reduces the noise we see when we place
4 these sensors in the rat jugular. (b) To illustrate this, here we have monitored plasma
5 vancomycin concentrations after a 30 mg/kg intravenous injection. The baseline noise decreases
6 from 2.3% when the counter electrode is enclosed in the catheter to 0.8% in the new
7 architecture, which converts to standard deviations in concentration of 3.5 μM and 1.0 μM
8 respectively. (c) Looking closely at the square wave voltammograms, we see that there is a
9 reduction in noise associated with the animal's pulse.
10
11
12

13
14 Extending the counter electrode outside of the catheter improves the signal-to-noise of intravenous
15 EAB sensors. To illustrate this, we monitored plasma vancomycin levels upon a 30 mg/kg
16 intravenous dose using both our initial architecture and the above-described, new architecture (Fig.
17 6a). The 1.0 μM noise (defined as the standard deviations of the fluctuations around the baseline
18 prior to dosing) associated with the new architecture under these experimental conditions is
19 approximately 3 times smaller than that we see for our first bundled architecture (Fig. 6b). One
20 source of this discrepancy is the fact that voltammograms collected in the rat jugular using this
21 new architecture exhibit less noise associated with the heartbeat (Fig. 6c). Given the results
22 reported here, we suspect that this noise occurs as the animal's pulse dilates and constricts the vein
23 and, thus, the catheter, causing the R_s to vary periodically for our first bundled architecture.
24
25
26
27
28
29
30
31

32
33 The effects we observe may be relevant to 3-electrode EAB sensor deployments beyond the
34 bundled intravenous sensors explored here. For example, there has been growing interest in less-
35 invasive EAB sensors deployed as subdermal or intradermal microneedles.^{21,22} In these scenarios,
36 there is limited liquid or limited electrolyte present, which could similarly lead to high resistances
37 between the counter electrode and working electrode. Consistent with our findings, as a result of
38 the limited electrolyte present, others have measured high signal to noise when such EAB sensors
39 are placed in the dermal tissue of a rat,²¹ suggesting that reducing the resistance between the
40 working and counter electrodes could improve the performance of such sensors.
41
42
43
44
45
46
47

48 **Conclusions.** Here we have shown that changing the relative placements of their three electrodes
49 can significantly improve the performance of catheter-bound in-vivo sensors. Specifically, the
50 voltammogram baselines were lower and peak heights higher for architectures in which the counter
51 electrode emerges from the lumen of the catheter. We attribute this difference to a reduction in the
52 resistance between the working electrode and counter electrodes. We have also shown that the
53
54
55
56
57
58
59
60

1
2
3 EAB counter electrode can be significantly smaller than the working electrode without harming
4 sensor performance. Finally, we combined these two observations to create a new, intravenous
5 EAB sensor architecture that achieves significantly improved performance when placed in the
6 jugular veins of live rats.
7
8
9

10 11 12 **Acknowledgements**

13
14 The in-vivo experiments were aided by J. Gibson and K. Honeywell, who helped with monitoring
15 and termination for multiple in-vivo experiments. The primary author greatly thanks K. Son for
16 helping accurately diagnose the cause of the shorting. Advice, feedback and general
17 electrochemical knowledge was supplemented by Prof. L. Sepunaru. This work was supported by
18 the NIH (R01AI145206), by the Office of Naval Research (N00014-20-1-2164), by the Otis
19 Williams Postdoctoral Fellowship Fund (KL) and the Department of Defense through the National
20 Defense Science and Engineering Graduate Fellowship (NE).
21
22
23
24
25
26
27
28
29
30

31 **References**

- 32
33 (1) Dauphin-Ducharme, P.; Yang, K.; Arroyo-Currás, N.; Ploense, K. L.; Zhang, Y.; Gerson,
34 J.; Kurnik, M.; Kippin, T. E.; Stojanovic, M. N.; Plaxco, K. W. Electrochemical Aptamer-
35 Based Sensors for Improved Therapeutic Drug Monitoring and High-Precision, Feedback-
36 Controlled Drug Delivery. *ACS Sensors* **2019**, *4* (10), 2832–2837.
37 <https://doi.org/10.1021/acssensors.9b01616>.
38
39 (2) Arroyo-Currás, N.; Somerson, J.; Vieira, P. A.; Ploense, K. L.; Kippin, T. E.; Plaxco, K.
40 W. Real-Time Measurement of Small Molecules Directly in Awake, Ambulatory
41 Animals. *Proc. Natl. Acad. Sci. U. S. A.* **2017**, *114* (4), 645–650.
42 <https://doi.org/10.1073/pnas.1613458114>.
43
44 (3) Dauphin-Ducharme, P.; Plaxco, K. W. Maximizing the Signal Gain of Electrochemical-
45 DNA Sensors Graphical Abstract HHS Public Access. *Anal Chem* **2016**, *88* (23), 11654–
46 11662. <https://doi.org/10.1021/acs.analchem.6b03227>.
47
48 (4) Ferguson, B. S.; Hoggarth, D. A.; Maliniak, D.; Ploense, K.; White, R. J.; Woodward, N.;
49 Hsieh, K.; Bonham, A. J.; Eisenstein, M.; Kippin, T. E.; Plaxco, K. W.; Soh, H. T. Real-
50
51
52
53
54
55
56
57
58
59
60

- 1
2
3 Time, Aptamer-Based Tracking of Circulating Therapeutic Agents in Living Animals. *Sci.*
4 *Transl. Med.* **2013**, *5* (213). <https://doi.org/10.1126/scitranslmed.3007095>.
- 5
6 (5) Plaxco, K. W.; Idili, A.; Gerson, J.; Kippin, T. Seconds-Resolved, in Situ Measurements
7 of Plasma Phenylalanine Disposition Kinetics in Living Rats. *Anal. Chem.* **2021**, *93* (8),
8 4023–4032. <https://doi.org/10.1021/acs.analchem.0c05024>.
- 9
10 (6) Idili, A.; Arroyo-Currás, N.; Ploense, K. L.; Csordas, A. T.; Kuwahara, M.; Kippin, T. E.;
11 Plaxco, K. W.; Arroyo-Curras, N.; Ploense, K. L.; Csordas, A. T.; Kuwahara, M.; Kippin,
12 T. E.; Plaxco, K. W. Seconds-Resolved Pharmacokinetic Measurements of the
13 Chemotherapeutic Irinotecan: In Situ in the Living Body. *Chem. Sci.* **2019**, *10* (35), 8164–
14 8170. <https://doi.org/10.1039/c9sc01495k>.
- 15
16 (7) Das, J.; Cederquist, K. B.; Zaragoza, A. A.; Lee, P. E.; Sargent, E. H.; Kelley, S. O. An
17 Ultrasensitive Universal Detector Based on Neutralizer Displacement. *Nat. Chem.* **2012**.
18 <https://doi.org/10.1038/nchem.1367>.
- 19
20 (8) Patolsky, F.; Weizmann, Y.; Willner, I. Redox-Active Nucleic-Acid Replica for the
21 Amplified Bioelectrocatalytic Detection of Viral DNA. *J. Am. Chem. Soc.* **2002**.
22 <https://doi.org/10.1021/ja0119752>.
- 23
24 (9) Hansen, J. A.; Mukhopadhyay, R.; Hansen, J.; Gothelf, K. V. Femtomolar
25 Electrochemical Detection of DNA Targets Using Metal Sulfide Nanoparticles. *J. Am.*
26 *Chem. Soc.* **2006**, *128* (12), 3860–3861. <https://doi.org/10.1021/ja0574116>.
- 27
28 (10) Gooding, J. J. Electrochemical DNA Hybridization Biosensors. *Electroanalysis*. 2002.
29 [https://doi.org/10.1002/1521-4109\(200209\)14:17<1149::AID-ELAN1149>3.0.CO;2-8](https://doi.org/10.1002/1521-4109(200209)14:17<1149::AID-ELAN1149>3.0.CO;2-8).
- 30
31 (11) Arroyo-Currás, N.; Dauphin-Ducharme, P.; Ortega, G.; Ploense, K. L.; Kippin, T. E.;
32 Plaxco, K. W. Subsecond-Resolved Molecular Measurements in the Living Body Using
33 Chronoamperometrically Interrogated Aptamer-Based Sensors. *ACS SENSORS* **2018**, *3*
34 (2), 360–366. <https://doi.org/10.1021/acssensors.7b00787>.
- 35
36 (12) Arroyo-Currás, N.; Ortega, G.; Copp, D. A.; Ploense, K. L.; Plaxco, Z. A.; Kippin, T. E.;
37 Hespanha, J. P.; Plaxco, K. W. High-Precision Control of Plasma Drug Levels Using
38 Feedback-Controlled Dosing. *ACS Pharmacol. Transl. Sci.* **2018**, *1* (2), 110–118.
39 <https://doi.org/10.1021/acsptsci.8b00033>.
- 40
41 (13) Rawson, T. M.; O'Hare, D.; Herrero, P.; Sharma, S.; Moore, L. S. P.; de Barra, E.;
42 Roberts, J. A.; Gordon, A. C.; Hope, W.; Georgiou, P.; Cass, A. E. G.; Holmes, A. H.
- 43
44
45
46
47
48
49
50
51
52
53
54
55
56
57
58
59
60

- 1
2
3 Delivering Precision Antimicrobial Therapy through Closed-Loop Control Systems. *J.*
4 *Antimicrob. Chemother.* **2018**. <https://doi.org/10.1093/jac/dkx458>.
5
6
7 (14) Downs, A. M.; Gerson, J.; Hossain, M. N.; Ploense, K.; Pham, M.; Kraatz, H. B.; Kippin,
8 T.; Plaxco, K. W. Nanoporous Gold for the Miniaturization of in Vivo Electrochemical
9 Aptamer-Based Sensors. *ACS Sensors* **2021**, *6* (6), 2299–2306.
10 https://doi.org/10.1021/ACSSENSORS.1C00354/SUPPL_FILE/SE1C00354_SI_001.PDF
11
12
13
14 .
15 (15) Chung, J.; Sepunaru, L.; Plaxco, K. W. On the Disinfection of Electrochemical Aptamer-
16 Based Sensors. *ECS Sensors Plus* **2022**, *1* (1), 011604. [https://doi.org/10.1149/2754-](https://doi.org/10.1149/2754-2726/ac60b2)
17 [2726/ac60b2](https://doi.org/10.1149/2754-2726/ac60b2).
18
19
20 (16) Bard, Allen J., Faulkner, L. Double-Layer Capacitance and Charging Current in
21 Electrochemical Measurements. In *Electrochemical Methods: Fundamentals and*
22 *Applications*; 2001; pp 14–18.
23
24
25 (17) Bard A. J., F. L. R. TECHNIQUES BASED ON CONCEPTS OF IMPEDANCE. In
26 *Electrochemical Methods: Fundamentals and Applications*; 2001; pp 368–416.
27
28
29 (18) Westbrook, P. Analytical Electrochemistry in Textiles. In *Woodhead Publishing*;
30 Woodhead Publishing, 2005; pp 3–36. <https://doi.org/10.1533/9781845690878.1.1>.
31
32 (19) Elgrishi, N.; Rountree, K. J.; McCarthy, B. D.; Rountree, E. S.; Eisenhart, T. T.;
33 Dempsey, J. L. A Practical Beginner's Guide to Cyclic Voltammetry. *J. Chem. Educ.*
34 **2018**, *95* (2), 197–206. <https://doi.org/10.1021/acs.jchemed.7b00361>.
35
36
37 (20) Ciobanu, M.; Wilburn, J. P.; Krim, M. L.; Cliffel, D. E. Fundamentals. In *Handbook of*
38 *Electrochemistry*; Elsevier, 2007; pp 3–29. [https://doi.org/10.1016/B978-044451958-](https://doi.org/10.1016/B978-044451958-0.50002-1)
39 [0.50002-1](https://doi.org/10.1016/B978-044451958-0.50002-1).
40
41
42
43 (21) Wu, Y.; Tehrani, F.; Teymourian, H.; Mack, J.; Shaver, A.; Reynoso, M.; Kavner, J.;
44 Huang, N.; Furnidge, A.; Duvvuri, A.; Nie, Y.; Laffel, L. M.; Doyle, F. J.; Patti, M. E.;
45 Dassau, E.; Wang, J.; Arroyo-Currás, N. Microneedle Aptamer-Based Sensors for
46 Continuous, Real-Time Therapeutic Drug Monitoring. *Anal. Chem.* **2022**, *94* (23), 8335–
47 8345. <https://doi.org/10.1021/acs.analchem.2c00829>.
48
49
50
51 (22) Lin, S.; Cheng, X.; Zhu, J.; Wang, B.; Jelinek, D.; Zhao, Y.; Wu, T. Y.; Horrillo, A.; Tan,
52 J.; Yeung, J.; Yan, W.; Forman, S.; Coller, H. A.; Milla, C.; Emaminejad, S. Wearable
53 Microneedle-Based Electrochemical Aptamer Biosensing for Precision Dosing of Drugs
54
55
56
57
58
59
60

1
2
3
4
5
6
7
8
9
10
11
12
13
14
15
16
17
18
19
20
21
22
23
24
25
26
27
28
29
30
31
32
33
34
35
36
37
38
39
40
41
42
43
44
45
46
47
48
49
50
51
52
53
54
55
56
57
58
59
60

with Narrow Therapeutic Windows. *Sci. Adv.* **2022**, 8 (38), eabq4539.
https://doi.org/10.1126/SCIADV.ABQ4539/SUPPL_FILE/SCIADV.ABQ4539_SM.PDF.